Pure & Appl. Chem., Vol. 56, No. 11, pp 1555-1567, 1984.
Printed in Great Britain.

033-4545/84 $3.00 + 0.00
Pergamon Press Ltd.

LASER DIAGNOSTICS OF MATERIALS AND CHEMISTRY

Allen Hartford Jr.

Chemistry Division, Los Alamos National Laboratory, Los Alamos, NM 87545, USA

Abstract - Recent developments in laser-based spectroscopic techniques posessing high spatial, temporal, and spectral resolution have provided the capability to perform noninvasive, in situ monitoring of chemical and physical phenomena. These laser diagnostics have been widely applied to high-temperature processes allowing a diversity of measurements to be made, from qualitative and quantitative detection of high-temperature species to measurement of the temperature dependence of elementary rate constants.

INTRODUCTION

Substantial effort has been directed toward understanding high temperature phenomena. A particularly challenging problem has been to characterize the chemical and physical processes which occur at elevated temperatures and are not predictable by extrapolation from lower temperature data. In recent years the study of high temperature processes has been facilitated by developments in instrumentation and measurement techniques. Among the promising diagnostic methods that have emerged are those based on advances in laser spectroscopy. Numerous laser-based diagnostic techniques have been demonstrated that simultaneously provide high spatial, temporal, and spectroscopic resolution and, perhaps more importantly, allow nonintrusive interrogation of the systems under investigation. These attributes have permitted real-time in situ detection and measurement of atomic and molecular species in such hostile environments as flames,[1-8] internal combustion engines,[9,10] plasmas,[11,12] and coal gasifiers.[13] In addition, laser techniques have proven quite versatile for studying the kinetics and mechanisms of chemical reactions.[14-20] Species typically encountered in high temperature processes can be readily produced under well-controlled conditions by laser photolysis of suitable materials. The subsequent temporal evolution of the species thus produced may then be followed by various laser diagnostics. This approach has yielded much fundamental information concerning state-selected chemical reactions. Yet other novel laser techniques have been used to study molecular ions[21-23] and metal clusters,[24-26] species often present in high temperature processes.

The number of laser diagnostics and their applications to high-temperature processes are far too vast to review in the present discussion. Rather by describing some recent investigations, the versatility of laser diagnostics and their possible extension to other applications will be apparent.

APPLICATION OF LASERS TO CHEMICAL ANALYSIS

One of the basic challenges of high-temperature science is to understand the chemical composition of systems under extreme conditions. Sampling techniques coupled with conventional analytical procedures (e.g. gas chromatography, absorption spectroscopy, wet chemistry) often fail to provide adequate spatial and temporal information. As a consequence, much vital information concerning concentration fluctuations and the presence of unusual intermediates can be lost.

Significant advances in the ability to make noninvasive in situ measurements with excellent spatial and temporal resolution have resulted from the development of laser spectroscopic techniques. Among the laser diagnostic techniques that possess these attributes and that have been successfully applied in a number of applications are laser-induced fluorescence (LIF), laser-induced breakdown spectroscopy (LIBS),[27,28] and coherent anti-Stokes Raman scattering (CARS) and its variants such as BOXCARS.[29] To date these techniques have been primarily employed to monitor gaseous media, although examples of applications to liquids and solids also exist. The predominant high-temperature application of laser diagnostics has been in the study of combustion phenomena.

Recently, we have evaluated and tested several laser diagnostics for on-line chemical analysis in two rather different industrial processes: coal gasification and steel production. In the former application there is need to rapidly monitor the product gas to ensure that it is of the appropriate composition (i.e., is of the correct heating value) and that toxic or corrosive contaminants have been reduced to acceptable levels. During the manufacture of steel rapid on-line analysis would improve productivity, lead to better consistency in product quality, and result in reduced energy consumption.

Real-time, full-flow monitoring of the composition of coal gasifier streams poses a severe test of optical instrumentation. Depending on the particular gasification process involved, pressures typically exceed 10 atm, temperatures of 1000 K are common, and the gas streams can be ladened with particulates and heavy hydrocarbons (tars). Consequently, optical transmission and resulting signal levels can be severely degraded. In spite of these limitations a CARS apparatus has been successfully implemented on a stirred, fixed-bed coal gasifier located at the Morgantown Energy Technology Center (METC) in Morgantown, West Virginia. Both major and minor constituents of the process stream were measured in real-time (~2-s temporal resolution). In addition LIBS has been used to identify numerous corrosive and toxic elements within the gasifier process stream. By virtue of the rapid temporal response of these diagnostics, both may ultimately have application to active control of the gasification and cleanup processes.

Coherent anti-Stokes Raman scattering is a four-wave mixing process that occurs when two incident laser beams interact through the third-order nonlinear susceptibility of a material and produce coherent radiation at a frequency $\omega_3 = 2\omega_1 - \omega_2$.[30] The frequencies ω_1 and ω_2 are generally referred to as the pump and Stokes frequencies, respectively. When the frequency difference between ω_1 and ω_2 corresponds to the frequency of a Raman-active mode in the material being probed, a resonant enhancement occurs. The CARS process is an intensity-dependent effect, being proportional to $I_1^2 I_2$, where I_1 and I_2 are the intensities of the beams at ω_1 and ω_2, respectively. Because of this intensity dependence, most CARS studies have been performed with pulsed lasers. A diagram of a typical CARS monitoring system is shown in Fig. 1. The pump wavelength (532 nm) is the frequency-doubled output from a pulsed Nd:YAG laser. A portion of the 532-nm beam is used to pump a tunable dye laser which provides the Stokes beam.

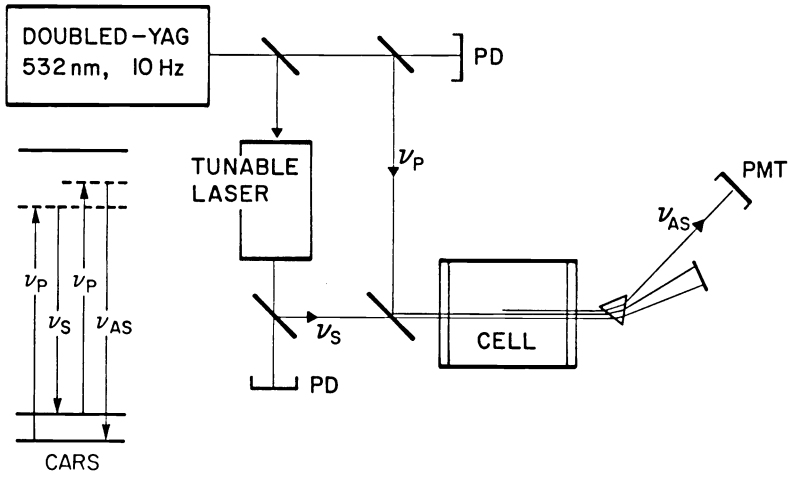

Fig. 1. Schematic of a typical apparatus for CARS measurments. A portion of the frequency-doubled output (532 nm) of a Nd:YAG laser provides the pump beam (ν_p), while the remainder pumps a dye laser which provides the Stokes beam (ν_s).

Our CARS measurements on the METC gasifier were made at a location immediately following the reaction vessel and a cyclone separator. At this location the gas stream was at high-temperature and high-pressure and contained significant levels of tars and particulates. This environment resulted in strong optical scattering of the laser beams which precluded a measurement of the absolute energy in the anti-Stokes beam (ω_{as}). As a consequence, we were only able to measure relative molecular densities by separating the anti-Stokes beam from the input beams using a 0.5-m monochromator. Ratios of concentrations were determined relative to N_2, a gasifier constituent which due to its chemical inertness is not expected to vary.

The CARS signals from N_2 and CO in the METC gasifier are shown in Figs. 2 and 3, respectively. In each case the spectra on the right were obtained by scanning the tunable dye laser through the band contour, while the signals on the left were obtained as a function of time with the dye laser fixed at the CARS peak. To obtain the ratio of CO to N_2 from the

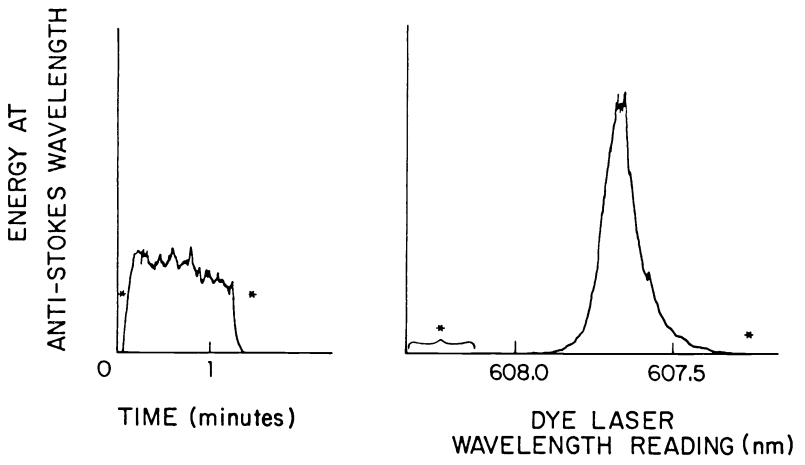

Fig. 2. The CARS signal of N_2 present in the METC stirred, fixed-bed coal gasifier. The spectrum on the right was obtained by scanning the tunable dye laser over the entire band contour. The signal on the left corresponds to the peak CARS signal as a function of time.

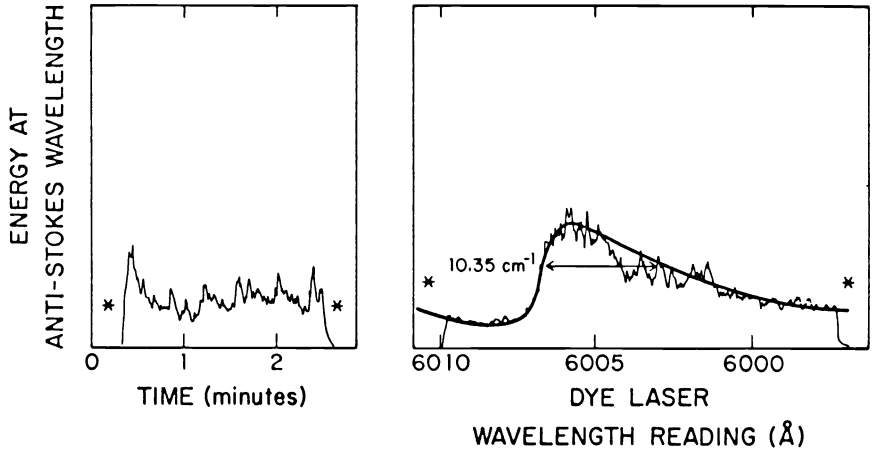

Fig. 3. The CARS signal of CO present in the METC coal gasifier. The spectrum on the right is a scan over the entire band contour, while the signal on the left was obtained by monitoring the peak CARS signal as a function of time.

CARS data, it was necessary to estimate the CARS susceptibilities from tabulated spontaneous Raman line strengths and the linewidths obtained from the gasifier scans. The relationship is given by

$$\frac{\chi(CO)}{\chi(N_2)} \sim \frac{S(CO)/\Delta\nu(CO)}{S(N_2)/\Delta\nu(N_2)} \quad , \qquad (1)$$

where χ is the susceptibility, S the spontaneous Raman line strength, and $\Delta\nu$ the linewidth. The concentration ratio obtained in this manner was $[CO]/[N_2] = 0.34$. In an independent gas chromatographic (gc) measurement the N_2 concentration was found to be 48%, which upon substitution in our ratio yields a CO concentration of 17%. The gc value for CO was 23%. Sources of uncertainties in the CARS determination include temporal fluctuations in the peak CARS signals and variations in the CARS linewidths.

Comparison of the time behavior of the peak CARS signals of CO and N_2 reveals that CO signal fluctuations are twice as large as those observed for N_2. Since the signal-to-noise ratio should be comparable in both cases, it appears that the CO fluctuations are indicative of true concentration fluctuations.

In addition to N_2 and CO, H_2S and CH_4 have been detected in the METC gasifier. The CARS signal from H_2S is shown in Fig. 4, from which a concentration of 0.22% was computed. The methane signal is displayed in Fig. 5. The CH_4 CARS spectrum exhibits the prominent

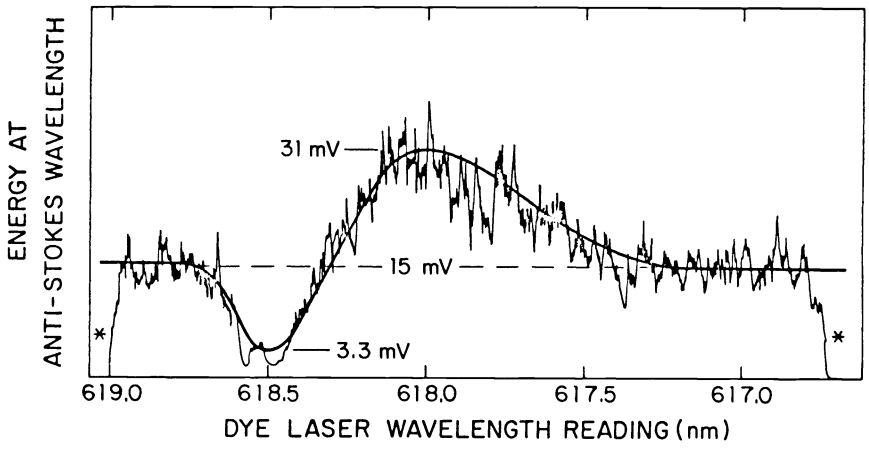

Fig. 4. The CARS spectrum of H_2S present in the METC coal gasifier.

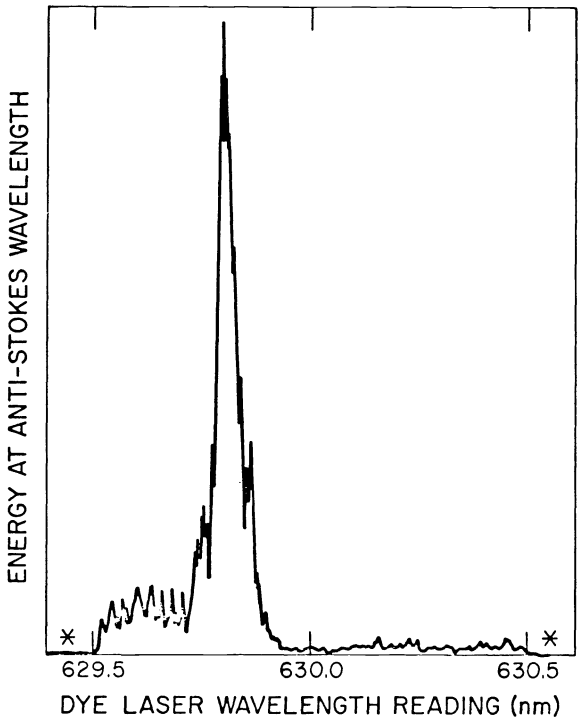

Fig. 5. The CARS spectrum of CH_4 present in the METC coal gasifier. The smaller red-shifted feature appears to be a hot-band transition.

Q-branch, as well as a red-shifted tail. The frequency of the tail correlates well with an expected hot band [(0,0,0,1) → (1,0,0,1)], but the shape is not as anticipated. The CH_4 hot band may provide a straightforward method for temperature measurement. Most temperature determinations by CARS have utilized comparisons between experimental and computer simulated N_2 band contours,[31,32] an approach that works well at pressures up to 1 atm. However, at higher pressures for which pressure-broadened widths of Q-branch rotational lines become comparable to their spacing, collisional narrowing occurs.[33] As a consequence of this phenomenon, at pressures up to 100 atm the overall Q-branch width does not change appreciably. Furthermore, neither the theory for collisional narrowing nor the CARS data base have been extended to high pressure and temperature conditions. Consequently, it is not yet possible to derive accurate gasifier temperatures from the N_2 CARS spectra. We plan to evaluate temperature measurements based on both the N_2 rotational structure and the CH_4 vibrational structure.

Historically, the presence of certain toxic and corrosive materials (Na, K, Ba, Ca, Mg, Se, As, Cd, Pb, etc.) in the process streams of coal gasifiers has been difficult to detect. Furthermore, the form in which these materials exist (i.e. elemental, molecular, or contained in particulates) in many cases is not well established. In the combustion of coal-derived gas to drive turbines, gas-solid corrosion reactions can result in severe damage to the turbine blades if elements such as the alkali metals are not maintained at acceptable levels.

Laser-induced breakdown spectroscopy has proven to be a versatile technique for monitoring toxic and corrosive materials in coal gasifiers. In LIBS, the output beam of a pulsed laser is focused into the material under investigation. At sufficiently high irradiances (10^8 - 10^9 W/cm^2 for air at atmospheric pressure) a dielectric breakdown occurs and a luminous plasma is produced. Molecules and aerosols in the plasma volume are reduced to highly excited atoms. It is the characteristic emission spectra that permits detection and indentification of particular atoms.

A schematic of a typical LIBS apparatus is shown in Fig. 6. The plasma is generated by the focused output of a Nd:YAG laser. The emission from the plasma is dispersed and detected with a spectrometer equipped with a time-gated diode array. The gating allows introduction of a time-delay between plasma initiation and spectral recording which results in an improved signal-to-noise ratio (SNR). The early portion of the plasma is dominated by a strong continuum emission which decays rapidly. On the other hand, emission from neutral atoms persists for a much longer time. Consequently, by delaying observation until the continuum has decayed in intensity provides a substantial enhancement of the SNR.

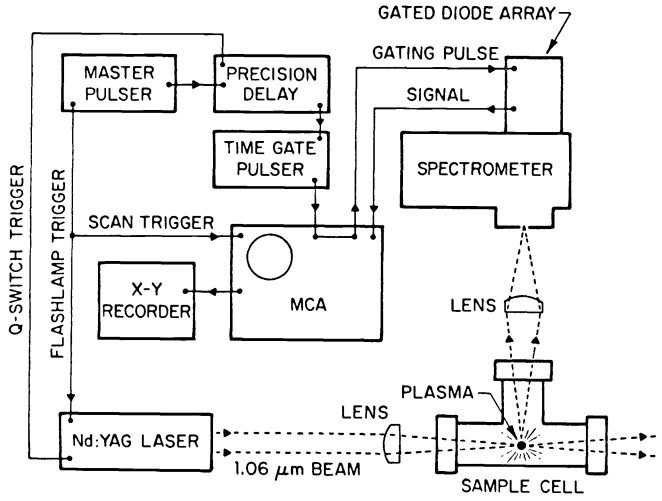

Fig. 6. Apparatus for performing time-resolved laser-induced breakdown spectroscopy. The time-gated diode array allows spectral recording to be delayed with respect to the onset of breakdown. The signal-to-noise ratio can be improved using this procedure.

A LIBS apparatus was installed on the METC coal gasifier. A single-ended optical configuration was employed in which a mirror placed at 45° with respect to the laser beam both transmitted the 1.06-μm radiation and imaged the breakdown spot on the spectrometer slit. Spectra were recorded over the spectral interval from 300 nm to 900 nm. Typical spectra are shown in Figs. 7 and 8. Analysis of the spectra revealed that emission from C, H, O, N, Cr, Cu, Fe, Mg, Pb, S, and Se was consistently reproducible and exhibited many-line signatures. Emission from the elements K, Ca, Cd, Mn, Al, Ba, and Li was observed only periodically. This latter behavior was suggestive of breakdown of particulates which traverse the laser focal volume on a random basis.

The current method for determining the composition of a steel melt utilizes conventional spark spectroscopy. A sample is withdrawn from the melt, allowed to solidify, and finally incorporated as an electrode in a conventional spark source. The elapsed time between sample extraction and quantitative analysis by spark spectroscopy is typically 5 to 10 minutes. Our goal is to reduce the analysis time to less than one minute.

The concept of using lasers for rapid on-line spectrochemical analysis of metal samples was initially explored during the 1960's.[34,35] Although some investigations have involved probing the surface of molten metal directly,[36] this approach appears to have some practical difficulties for on-line analysis of steel samples. One problem simply involves optical

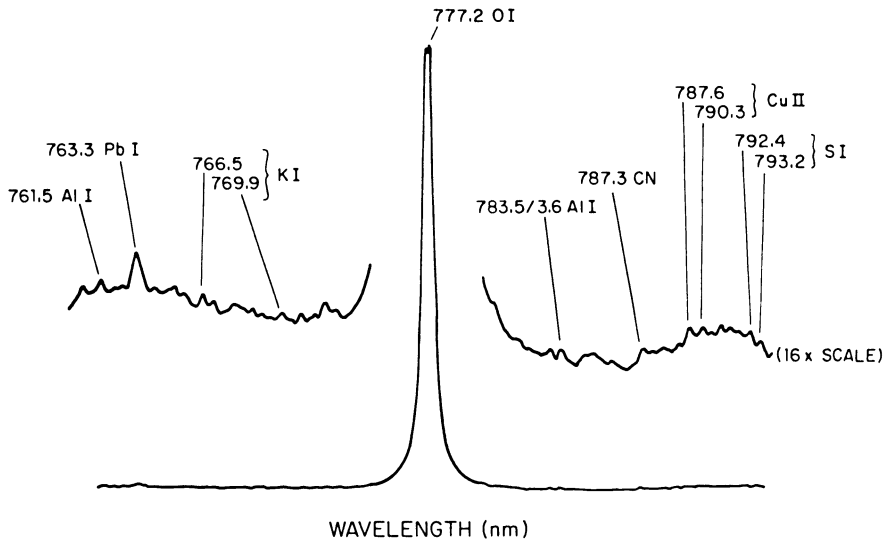

Fig. 7. A typical LIBS spectrum obtained from the output gas stream of the METC coal gasifier showing the trace elements Al, Cu, K, Pb, and S.

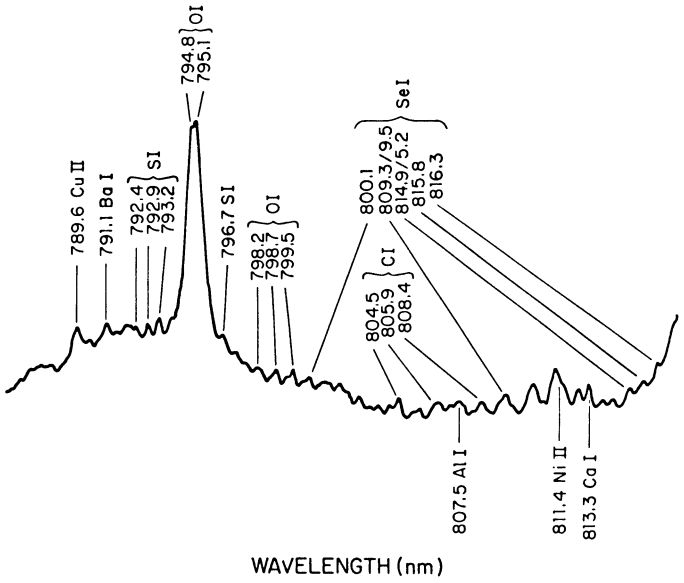

Fig. 8. A LIBS spectrum from the process stream of the METC coal gasifier showing the trace elements Al, Ba, Ca, Cu, S, and Se.

access to the surface of the molten steel which is covered by a layer of slag. Even if a direct surface probe could be designed, the vapor above the surface could have a different composition then the melt, thereby distorting the analysis. Consequently, we have chosen an approach that involves rapidly extracting a sample and allowing it to solidify prior to analysis. Two alternative analytical procedures are being evaluated, one using a direct breakdown on the metal surface, the other employing a laser to merely generate a fine aerosol which is then transported by a carrier gas to an inductively coupled plasma (ICP) for spectral analysis.

The apparatus used for direct spark analysis using LIBS is depicted in Fig. 9. Initially calibration curves were obtained by irradiating steel samples containing a known amount of the element of interest and plotting the emission intensity from a particular atomic transition versus concentration. As an example, six samples of steel containing differing amounts of sulfur were analyzed five times each. Relative standard deviations were calculated

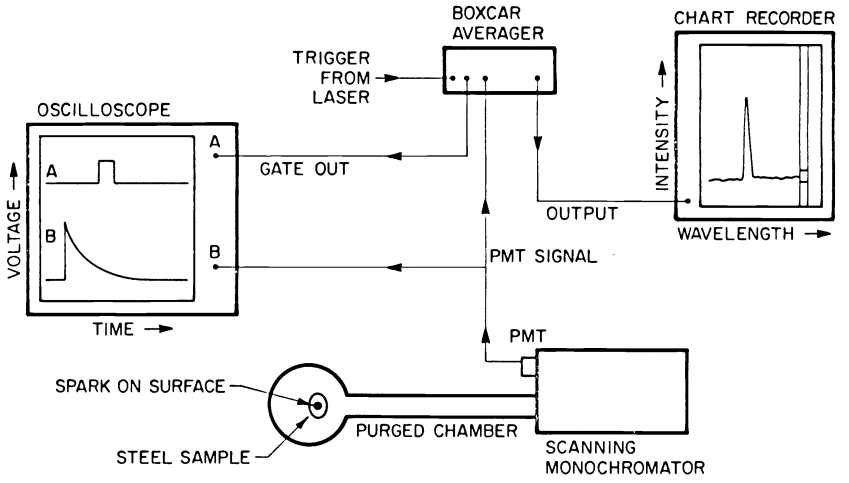

Fig. 9. Apparatus for LIBS elemental analysis of solid steel samples. A spark is generated by a Nd:YAG laser and the emission is dispersed by a scanning monochromator.

and found to range from 28% at 0.033% sulfur to 5.7% at sulfur concentration of 0.52%. Using this approach curves were developed for a number of elements and the detection limits established. These are presented in Table I.

TABLE 1. Detection limits of elements important in steel obtained by direct laser-generated spark analysis.

Element	Detection Limit (%)
Carbon	0.054
Sulfur	0.03
Phosphorus	0.79
Molybdenum	>0.2
Manganese	0.2
Nickel	0.08
Chromium	0.067
Silicon	0.051
Titanium	0.01
Niobium	>0.066
Vanadium	0.022

The laser ablation of steel particles into an ICP for spectrochemical analyses has the potential for greater detection sensitivity than direct LIBS. The apparatus is shown in Fig. 10. A polychromator allows simultaneous monitoring of several elements. Calibration curves were developed in a manner similar to that used for LIBS, except that the emission intensity from the element of interest was ratioed to the intensity of a line emanating from singly ionized iron (271.4 nm). A typical calibration curve is shown in Fig. 11. Current detection limits using the laser ablation/ICP approach are provided in Table II. Comparison of these detection limits with those obtained by direct laser spark indicates that the laser ablation/ICP analysis in general provides a greater sensitivity. It should be noted that the detection limits obtained by both methods are preliminary and that further improvements are likely.

HIGH-TEMPERATURE CHEMICAL KINETIC MEASUREMENTS

Information concerning the temperature dependence of reaction rate constants is crucial for assessing the importance of various chemical reactions occurring in high-temperature processes. It is well known that an Arrhenius extrapolation of lower temperature data often fails to reproduce the observed high temperature behavior. Consequently, to permit reliable extrapolations the determination of rate constants over a meaningful temperature regime is necessary. Furthermore, since electronically or vibrationally excited species may react with

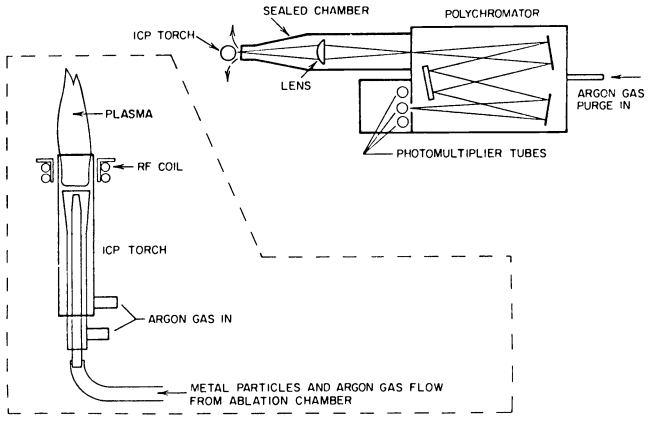

Fig. 10. Apparatus for elemental analysis of solid steel samples using laser ablation to produce metal particles which are entrained in an argon carrier gas and introduced into an inductively coupled plasma (ICP). The spectral emission from the ICP is analyzed by a polychromator capable of monitoring several elements simultaneously.

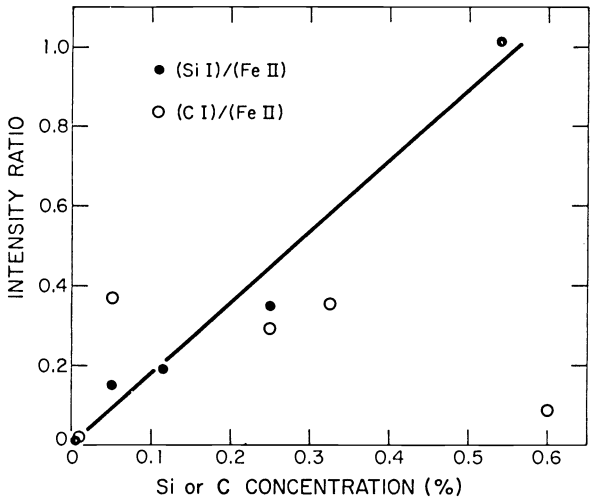

Fig. 11. Calibration curve for silicon using the laser ablation/ICP techniques. A comparable calibration curve for carbon could not be obtained due to impurities in the ICP carrier gas.

TABLE 2. Detection limits of elements important in steel obtained by laser ablation/ICP analysis.

Element	Detection Limit (%)
Sulfur	0.02
Phosphorus	0.25
Molybdenum	0.039
Manganese	0.2
Nickel	0.04
Chromium	0.067
Silicon	0.051
Titanium	0.02
Vanadium	0.022
Tin	0.01
Copper	0.038
Aluminum	0.009
Cobalt	0.014

different rates and produce different products than when in the ground state, state selective measurements are of importance.

The coupling of laser photolytic techniques for producing transient molecular species with highly sensitive laser-induced fluorescence (LIF) detection has permitted detailed kinetic studies of specific reactions under well-controlled conditions. A schematic diagram of a typical apparatus for performing such measurements is shown in Fig. 12. The species whose reactions we wish to study is generally produced by excimer laser photolysis of a suitable precursor molecule. A tunable probe laser is then used to excite fluorescence in the transient. Because the fluorescence intensity is proportional to the molecular concentration, by varying the delay time between the photolysis and probe laser pulses the temporal evaluation of the species concentration can be followed. In the presence of reactant gases this approach yields valuable kinetic information.

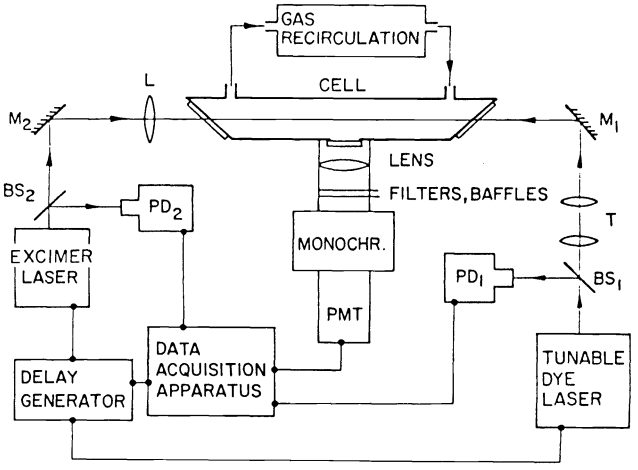

Fig. 12. Apparatus used to measure the rates of elementary chemical reactions. The excimer laser produces free radicals by laser photolysis of suitable precursor molecules. The tunable dye laser excites fluorescence in the free radicals. A variable delay between photolysis and probe laser allows temporal information to be obtained.

Recently, we have incorporated a high temperature cell into the laser photolysis/laser fluorescence apparatus. This cell (Fig. 13) is based on the design of Felder and coworkers[37] and is capable of operation in the range from 298-1300 K. A central high-purity alumina tube is heated resistively in two zones by Pt/40% Rh resistance wire. Thermal insulation is provided by an alumina heat shield surrounded by zirconia fiber insulation, with the whole assembly enclosed in a water-cooled brass vacuum chamber. The temperature is measured by thermocouples inserted through O-ring seals to probe various regions of the oven. The thermocouple outputs are sent to a Micricon microprocessor which automatically regulates the heater current. The reactant and buffer gases are introduced at the bottom of the cell and are heated as they flow slowly (~0.15 sℓm) through the center tube. A small amount of radical precursor in a helium mixture is introduced via a water-cooled variable length inlet system within a few centimeters of the optical ports to minimize pyrolysis and pre-reaction problems. The pressure is measured with a capacitance manometer and gas flows with calibrated Tylan mass flow meters. The gas flow in sufficiently fast to assure a fresh gas mix for each laser shot.

The initial reaction studied using the high temperature fluorescence cell involved that between C_2 and O_2. C_2 is known to exist in large concentrations in high temperature processes such as combustion. Furthermore, existence of a low lying electronic state ($a^3\Pi_u$) within 610 cm^{-1} of the ground state ($X^1\Sigma_g^+$)[38] means that both states will be populated at temperatures of interest.

Both $C_2(X^1\Sigma^+)$ and $C_2(a^3\Pi_u)$, henceforth denoted by $^1C_2$ and $^3C_2$, respectively, are produced upon the 193-nm multiple-photon dissociation of perfluorobutyne (CF_3CCCF_3). Addition of approximately 20 torr of He to the 1-2 mtorr of the precursor assures that the C_2 produced is

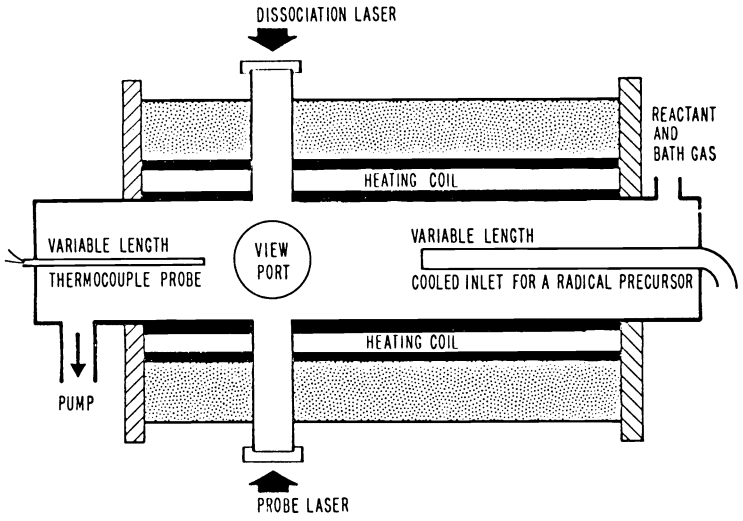

Fig. 13. High-temperature cell used to study the temperature dependence of the reaction rates of transient species.

translationally and rotationally thermalized. However, this pressure of helium does not effectively quench the vibrational excitation.

The $^3C_2$ was monitored by exciting the (0,0) band of the Swan bands ($d^3\Pi_g \leftarrow a^3\Pi_u$) at 516 nm and observing fluorescence from the (0,1) transition at 564 nm. Vibrationally excited $^3C_2$ was probed either by exciting the (v,v) transition in the Swan bands and monitoring fluorescence on the (v,v+1) band or by exciting the (v-1,v) band while detecting fluorescence from (v-1,v-1). To monitor the fate of $^1C_2$ we devised a novel double resonance scheme to excite fluorescence.[39] The approach involves initial excitation of the (3,0) band of the Phillips system ($A^1\Pi_u \leftarrow X^1\Sigma_g^+$) at 771 nm, followed 50 ns later by 404-nm excitation of the (2,3) band of the $C^1\Pi_u \leftarrow A^1\Pi_g$. Fluorescence is detected from the (2,1) band of the $C^1\Pi_u - A^1\Pi_g$ transition. This approach yields a much improved signal-to-noise ratio compared to simple excitation of and fluorescence detection from the Phillips system. This transition is weak and exhibits a radiative lifetime of 11 μs.[40] Furthermore, fluorescence is in the red where high temperature blackbody radiation is a major source of noise.

A typical example of the temporal behavior of $C_2(a^3\Pi_u, v=0)$ in the presence of oxygen is shown in Fig. 14. The long time decay exhibits single exponential behavior from which the disappearance rate of $^3C_2$ is obtained. The reaction rate constant at a particular temperature is derived by taking the slope from a Stern-Volmer plot of the disappearance rate versus O_2 pressure. Such a plot for a temperature of 886 K is shown in Fig. 15. Rate constants for v=0,1,2 of the $^3C_2$ state were determined at a number of temperatures. A logarithmic plot of the rate constants versus 1/T is shown in Fig. 16. An excellent fit of the v = 0 points to the Arrhenius expression, k(T) = A exp(-E/RT), was obtained with A = 1.49 ± 0.03 × 10^{-11} cm^3 $molecule^{-1}$ s^{-1} and E = 0.98 ± 0.02 kcal/mole. The data for the two excited vibrational levels of $^3C_2$ clearly do not reflect Arrhenius behavior, although the reaction rates appear to converge with that of v = 0 at higher temperatures. This behavior is consistent with the fact that at lower temperatures the vibrational relaxation of $C_2(a^3\Pi_u, v=1,2)$ dominates the kinetics while at elevated temperatures vibrational relaxation does not play as significant a role. A model which reproduces the early temporal behavior of the fluorescence signal (i.e. the risetime) and incorporates the reaction rate, singlet-triplet intersystem crossing rate, the initial relative $^3C_2/^1C_2$ quantum yields, and vibrational relaxation rates substantiates this argument.

The temperature dependence of the rate constants for the removal of $C_2(X^1\Sigma_g^+, v=0)$ by O_2 exhibits essentially the same Arrhenius behavior as the vibrationless triplet state. Previous experiments over the limited temperature range from 300-600 K were unable to determine unambiguously whether the reaction followed Arrhenius behavior or not.[14] Furthermore, the observed Arrhenius behavior was not predicted by a model proposed by other investigators.[17]

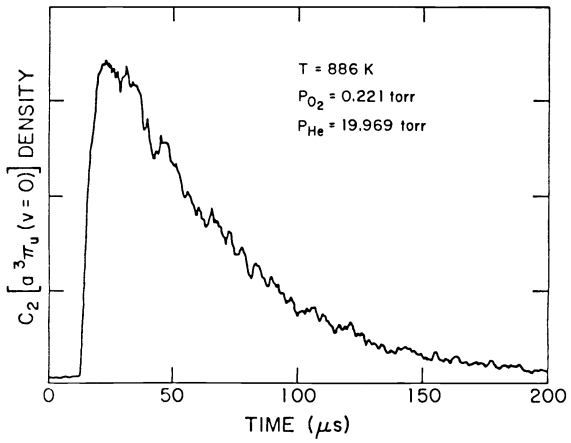

Fig. 14. Typical signal of the time dependence of the disappearance of $C_2((a^3\Pi_u, v=0)$ in the presence of a fixed pressure of O_2.

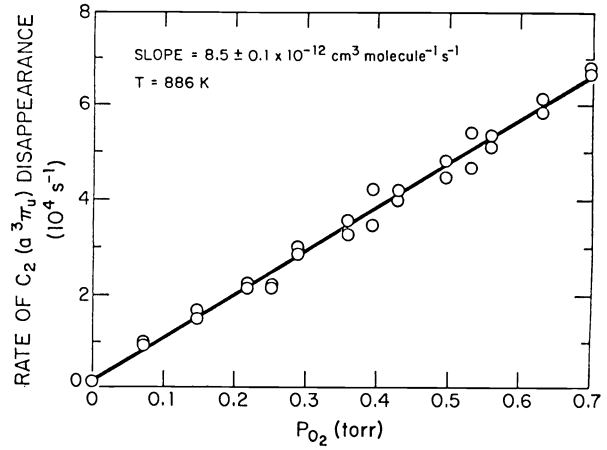

Fig. 15. The rate of ($C_2(a^3\Pi u$) disappearance as a function of O_2 pressure at 886 K. The slope of the line yields the reaction rate constant at this temperature.

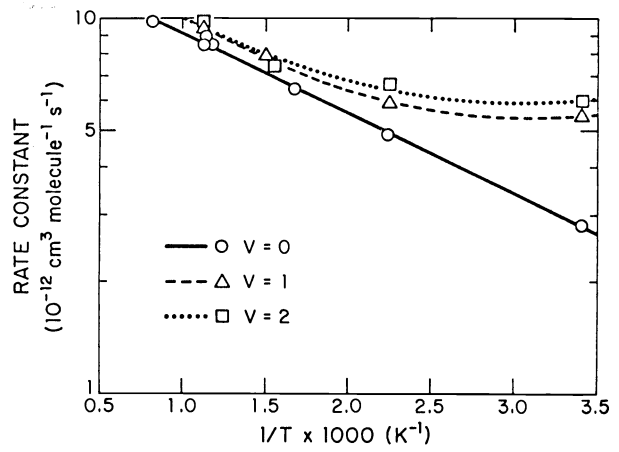

Fig. 16. The temperature dependence of the rate constant for the reaction of $C_2(a^3\Pi_u)$ with O_2. The reaction of the v=0 level exhibits Arrhenius behavior over the temperature range from 298-1300 K, while the v=1,2 levels do not.

In order to understand the observed behavior in the $C_2 + O_2$ system, the following kinetic scheme involving reaction and intersystem crossing is considered:

$$^1C_2 + O_2 \xrightarrow{k_1} \text{products} \qquad (2)$$

$$^3C_2 + O_2 \xrightarrow{k_3} \text{products} \qquad (3)$$

$$^3C_2 + O_2 \underset{k_r}{\overset{k_f}{\rightleftharpoons}} {}^1C_2 + O_2 \quad . \qquad (4)$$

Mangir et al. using the method of Laplace transforms have solved the differential equations corresponding to these reactions.[17] In addition they showed that at 300 K the intersystem crossing rate constant was much faster than the reaction rate constant. Under these circumstances the observed disappearance rate, k_{obs} for both $^1C_2$ and $^3C_2$ is given by

$$k_{obs} = \frac{k_1 + Sk_3}{1 + S} \quad , \qquad (5)$$

where S is the equilibrium constant,

$$S = \frac{k_r}{k_f} = \frac{g_3}{g_1} \exp(\Delta E_{13}/RT) \quad . \qquad (6)$$

Here ΔE_{13} is the singlet-triplet energy separation and g_3 and g_1 are the degeneracies of the triplet (6) and singlet (1) states, respectively. Because S varies substantially over the temperatures employed in the present study, the temperature dependence of the observed disappearance rate constant will be Arrhenius only if $k_1 = k_3$. Intuitively, this could indeed be the case if intersystem crossing (a spin-allowed process for C_2 and O_2) occurs upon long-range interaction, while reaction takes place upon closer approach.

SUMMARY

We have attempted to indicate by way of several examples the ability of laser-based diagnostic techniques to make noninvasive measurements in hostile environments. Using coherent anti-Stokes Raman scattering both majority and minority species concentrations, as well as temperature, have been measured in the hot, high-pressure, particle-laden stream of a coal gasifier. In addition, using LIBS numerous toxic and corrosive elements in the gasifier stream have been identified, but not yet quantified. Laser-based methods are also being applied to the rapid analysis of molten metal. In addition to providing the capability for making analytical determinations, laser techniques have been extensively employed to measure the rates of elementary chemical reactions. Recently, the temperature regime over which such measurements are possible has been expanded. Data dereived from these studies will aid significantly in the modeling of complex systems.

Although much of the laser diagnostic activity to date has involved investigations of the gas phase, significant information concerning heterogeneous phenomena can still be inferred. For instance, gas-solid reactions can manifest themselves as changes in vapor phase composition. Furthermore, in the future we expect expanded studies involving reactions of refractory metals (both atoms and clusters) and additional investigations of processes occurring at interfaces and on surfaces.

ACKNOWLEDGMENTS

It is a pleasure to acknowledge Drs. David Taylor, Richard Oldenborg, Steven Baughcum, Thomas Loree, David Cremers, Leon Radziemski, and Harold Dilworth for their outstanding efforts in carrying out the research described here. I also wish to thank Mr. Monty Ferris for his expert assistance in carrying out numerous field tests. The author is also indebted to the Morgantown Energy Technology Center for sponsoring and participating in the CARS and LIBS programs. Support of the program for the analysis of molten metal by the Department of Energy Office of Industrial Programs and the American Iron and Steel Institute is gratefully acknowledged. This work was performed under the auspices of the U. S. Department of Energy.

REFERENCES

1. W. R. Anderson, L. J. Decker, and A. J. Kotlar, Combust. Flame 48, 179 (1982).
2. P. A. Bonczyk and J. A. Shirley, Combust. Flame 34, 253 (1979).
3. A. P. Baronavski and J. R. McDonald, Appl. Optics 16, 1897 (1977).
4. A. P. Baronavski and J. R. McDonald, J. Chem. Phys. 66, 3300 (1977).
5. L. A. Rahn, L. J. Zych, and P. L. Mattern, Optics Commun. 30, 249 (1979).
6. L. E. Harris, Chem. Phys. Lett. 93, 335 (1982).
7. R. J. Hall, Combust. Flame 35, 47 (1979).
8. J. H. Bechtel and R. E. Teets, Appl. Optics 18, 4138 (1979).
9. D. Klick, K. A. Marko, and L. Rimai, Appl. Optics 20, 1178 (1981).
10. I. A. Stenhouse, D. R. Williams, J. B. Cole, and M. D. Swords, Appl. Optics 18, 3819 (1979).
11. W. J. Van den Hock and J. A. Visser, J. Phys. D: Appl. Phys. 14, 1613 (1981).
12. F. C. Jahoda, SPIE 288, 518 (1981).
13. D. J. Taylor, "CARS Concentration and Temperature Measurements in Coal Gasifiers," Appl. Optics (submitted for publication).
14. W. M. Pitts, L. Pasternack, and J. R. McDonald, Chem. Phys. 68, 417 (1982).
15. H. H. Nelson, L. Pasternack, J. R. Eyler, and J. R. McDonald, Chem. Phys. 60, 231 (1981).
16. M. N. R. Ashfold, M. A. Fullstone, G. Hancock, and G. W. Ketley, Chem. Phys. 55, 245 (1981).
17. M. S. Mangir, H. Reisler, and C. Wittig, J. Chem. Phys. 73, 829 (1980).
18. H. Reisler, M. Mangir, and C. Wittig, Chem. Phys. 47, 49 (1980).
19. H. Reisler, M. S. Mangir, and C. Wittig, J. Chem. Phys. 73, 2280 (1980).
20. J. E. Butler, L. P. Goss, M. C. Lin, and J. W. Hudgens, Chem. Phys. Lett. 63, 104 (1979).
21. C. S. Gudeman, M. H. Begeman, J. Pfaff, and R. J. Saykally, Phys. Rev. Lett. 50, 727 (1983).
22. M. A. Duncan, V. M. Bierbanm, G. B. Ellison, and S. R. Leone, J. Chem. Phys. 79, 5448 (1983).
23. D. R. Guyer, L. Hüwel, and S. R. Leone, J. Chem. Phys. 79, 1259 (1983).
24. J. B. Hopkins, P. R. R. Langridge-Smith, M. D. Morse, and R. E. Smalley, J. Chem. Phys. 78, 1627 (1983).
25. M. D. Morse, J. B. Hopkins, P. R. R. Langridge-Smith, and R. E. Smalley, J. Chem. Phys. 79, 5316 (1983).
26. D. E. Powers, S. G. Hansen, M. E. Geusic, D. L. Michalopoulos, and R. E. Smalley, J. Chem. Phys. 78, 2866 (1983).
27. L. J. Radziemski and T. R. Loree, Plasma Chem. Plasma Proc. 1, 281 (1981).
28. L. J. Radziemski, T. R. Loree, D. A. Cremers, and H. M. Nelson, Anal. Chem. 55, 1246 (1983).
29. A. C. Eckbreth, Appl. Phys. Lett. 32, 421 (1978).
30. J. J. Valentini, Spectrometric Techniques 4, Academic Press, New York (1984).
31. A. C. Eckbreth and R. J. Hall, Combust. Flame 36, 87 (1979).
32. A. C. Eckbreth, R. J. Hall, NBS Mater. Res. Symp. Charact. High Temp. Vapors Gases, 10th, Gaithersburg, Maryland (1978).
33. R. J. Hall, J. F. Verdieck, and A. C. Eckbreth, Optics Commun. 35, 69 (1980).
34. E. F. Runge, Bonfiglio, and F. R. Bryan, Spectrochim. Acta 22, 1678 (1966).
35. R. H. Scott and A. Strasheim, Spectrochim. Acta 25B, 311 (1970).
36. T. Ozaki, T. Takahashi, Y. Iwai, K. Gunji, and E. Sodo, Tetsu To Hagana 68, 872 (1982).
37. W. Felder, A. Fontijn, H. N. Volltraner, and D. R. Voohes, Rev. Sci. Instrum. 195 (1980).
38. K. P. Huber and G. Herzberg, Molecular Spectra and Molecular Structure IV. Constants of Diatomic Molecules, Van Nostrand Reinhold, New York, 1979.
39. S. L. Baughcum and R. C. Oldenborg, "A New High Temperature Diagnostic for $C^2(X^1\Sigma_g^+)$ to Study the Reaction Kinetics and Intersystem Crossing Rates of $C_2(X^1\Sigma_g^+)$ and $C_2(a^3\Pi_u)$ with O_2 in the 298-1300 K Temperature Range," Western States Section Meeting of the Combustion Institute, October 17-18, 1983, Los Angeles, California.
40. P. Erman, D. L. Lambert, M. Larsson, and Mannfors, Astrophys. J. 253, 983 (1982).